Intramolecular non-covalent interactions as a strategy towards controlled photoluminescence in copper(i) complexes

CrossMark
click for updates

Intramolecular non-covalent interactions as a strategy towards controlled photoluminescence in copper(I) complexes†

G. A. Filonenko,[a] R. R. Fayzullin[b] and J. R. Khusnutdinova*[a]

In this work, we describe a new strategy for designing photoluminescent Cu(I) complexes. At its core are simple cyclophane inspired N-donor ligands featuring intramolecular interactions between aromatic units within a single molecule. Variation of the steric bulk inflicted a change in intramolecular stacking distances that in turn affected the emission colour of copper(I) complexes tunable in a 0.5 eV range from green to red. As the interactions driving emission are confined to the single molecule, no intermolecular aggregation is required to enable photoluminescence in solution, pristine crystals, or solution-cast polymer films. A crystallographic study provides a link between the spatial proximity of the aromatic rings of the ligands (ranging from 3.349 to 3.731 Å) and the enhancement of emission efficiency, which increases dramatically from 0.02 to 0.78 at 296 K as the ring spacing contracts. Photophysical and theoretical analyses confirm the involvement of intramolecular interactions in the formation of the emissive state and describe the observed phenomena at the molecular level.

Introduction

The vast class of photoluminescent (PL) compounds holds great importance in modern technology. Comprised of purely organic molecules or transition metal complexes, luminescent compounds have found broad application in light emitting devices,[1] smart materials for sensing[2] and imaging.[3,4] As the demand for such emitters steadily grows, new strategies for designing PL materials and modulating their properties become increasingly important.

Conventional transition metal (TM)-based luminophores rely heavily on the use of π-extended ligands required to create the desired bandgap that facilitates excitation and emission. This design strategy yielded remarkably efficient PL complexes with recent examples including Ir,[5] Pt,[6,7] Zn,[8] and Au.[9] Since noble metals currently comprise the most abundant class of TM-based PL complexes, the search for a cheap yet efficient and sustainable alternative remains an important objective.[10]

Over the last two decades, Cu(I) complexes have been recognized as a sustainable alternative to noble metal-based PL materials.[11–14] These compounds include mono- and binuclear complexes with chelating phosphines,[15–18] mononuclear phenanthroline-[19–21] or diimine-based complexes[22] and trigonal complexes with NHC-based and amide-bound ligands.[23–29] Similar to the rest of the TM-based emitters, the control over emissive properties in Cu(I) compounds is typically achieved by tuning the electronic properties of their ligands[30,31] or addressing the ligand conformational dynamics.[32] This implies that the emission of TM-complexes mainly relies on covalent interactions within one molecule, while the intermolecular and non-covalent interactions typically remain unutilized.

One conceptually opposite approach for designing PL compounds makes use of the intermolecular non-covalent interactions. Coined in 2001 by Tang, this strategy is referred to as aggregation induced emission (AIE) and it exploits the intermolecular arrangement in solid or aggregated state to enable photoluminescence.[34,35] This arrangement can, for example, restrict the molecular motions responsible for non-radiative relaxation or induce photoluminescence in π–π stacked assemblies that emit when aggregated in contrast to the non-emissive isolated molecular state.

The AIE behaviour is not limited to organic dyes and can be found in TM complexes. For example, non-covalent interactions were found to contribute to emission of Zn, Au, Pt, Ir, Al and Cu compounds.[36–41] However, with very few exceptions,[42,43] the non-covalent interactions involved in modulating photoluminescence

[a] *Coordination Chemistry and Catalysis Unit, Okinawa Institute of Science and Technology, Graduate University, 1919-1 Tancha, Onna-son, Kunigami-gun, Okinawa 904-0495, Japan. E-mail: juliak@oist.jp*

[b] *A.E. Arbuzov Institute of Organic and Physical Chemistry, Kazan Scientific Center, Russian Academy of Sciences, Arbuzov Street, 8, Kazan 420088, Russian Federation*
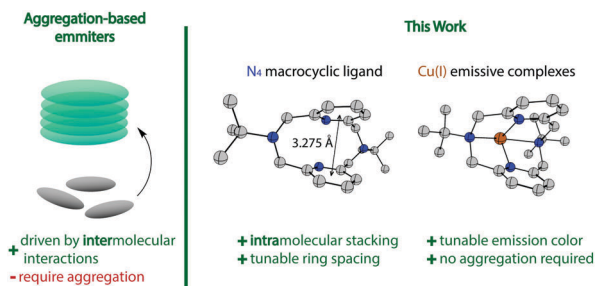
Fig. 1 Comparison between inter- and intramolecular interactions as the driving factor for photoluminescence. Structure of the **L1** pyridinophane macrocycle (N_4) adopted from ref. 33.

are intermolecular and therefore are highly sensitive to the structure of the bulk material and thus hard to control and translate to solution state.

Potentially one can overcome the limitations of the AIE approach if the non-covalent interactions driving the emission are intramolecular and therefore not affected by intermolecular arrangement. Such intramolecular interactions can be found in pyridinophane macrocycles (*e.g.* N,N'-dialkyl-2,11-diaza[3.3](2,6)-pyridinophane, Fig. 1). For example, the *N-tert*-butyl substituted pyridinophane ligand is conformationally flexible in transition metal complexes[44,45] and features a tight π–π spacing of 3.275 Å between two pyridine rings in the solid state in the free ligand (Fig. 1). If the interaction between non-conjugated pyridine rings can be utilized to enable emission in TM-complexes, the use of pyridinophane ligands would mark a conceptually new strategy for designing emissive TM complexes based on purely non-covalent interactions.

In this work, we demonstrate that such intramolecular interactions can be successfully employed to design a new class of photoluminescent Cu(I) complexes. The colour and quantum yield of the emission could be altered by controlling the conformation of the pyridinophane macrocyclic ligand by simply varying N-substituents (R group, Fig. 1). Namely, the variation of the spatial proximity of two non-conjugated pyridine rings within the macrocycle allowed for emission in a wide range of 524–665 nm with the quantum yield reaching 0.78 at room temperature. The photoluminescence of the complexes most emissive in the solid state was also successfully translated to dichloromethane solutions, thus overturning the prerequisite for emitters driven by the non-covalent interactions to be in the aggregated state.

Experimental section

All manipulations unless stated otherwise were performed using Schlenk or glovebox techniques under a dry argon atmosphere. Anhydrous solvents were dispensed from an MBRAUN solvent purification system and degassed prior to use. Anhydrous deuterated solvents were purchased from Eurisotop and stored over 4 Å molecular sieves. All chemicals unless noted otherwise were purchased from major commercial suppliers (TCI, Sigma-Aldrich and Nacalai Tesque) and used without purification.

Ligand **L1**,[33] 2,11-diaza[3.3](2,6)pyridinophane ($\mathbf{L_{NH}}$)[46] and NaBArF (sodium tetrakis[3,5-bis(trifluoromethyl) phenyl]borate)[47] were prepared according to literature procedures. $[Cu(MeCN)_4]^+$ precursors were prepared by dissolving Cu_2O in acetonitrile solutions in the presence of aqueous HBF_4 or HPF_6 followed by two consecutive recrystallizations from cold acetonitrile.[48]

Polymer blends of complexes **4–6** were prepared by mixing a saturated solution of 2–3 mg of the corresponding complex in CH_2Cl_2 with 1 mL of PMMA (poly(methyl methacrylate)) solution in CH_2Cl_2 containing *ca.* 100 mg of the polymer. The films were prepared from these blends by drop casting in a rectangular PTFE mold followed by drying *in vacuo*.

Instrumentation

NMR spectra were measured on JEOL ECZ600R 600MHz, JEOL ECZ400S 400 MHz and Bruker Avance II 400 MHz spectrometers. Full spectra are available in the ESI.† Electrospray ionization mass spectrometry (ESI-MS) measurements were performed on a Thermo Scientific ETD apparatus. Elemental analyses were performed using an Exeter Analytical CE440 instrument.

The photoluminescence measurements in degassed dichloromethane solutions at varying concentrations were performed using a Hitachi F7000 apparatus. Absorbance spectra were collected using an Agilent Cary 60 machine. Photoluminescence lifetime measurements were performed using the second harmonics of a Spectra-Physics Mai Tai pulsed laser and a Hamamatsu Photonics Streak Scope camera. The decay data were fitted with a single exponential decay function unless specified otherwise. The same laser light source equipped with a Thorlabs IS236A integrating sphere and an OceanOptics USB4000-ES spectrometer was used for quantum yield measurements in solutions (CH_2Cl_2, c = 0.5–1 μM) and in the solid state. The accuracy of quantum yield data was confirmed using a Hamamatsu Photonics Quantaurus-QY system that established the variations in absolute QY to be within 5% for solid and solution samples. Emission spectra were recorded using an OceanOptics USB4000-ES (solutions, Fig. 6B) or Hamamatsu Photonics Streak Scope camera (solids, Fig. 6A). The IR spectra were recorded using a Cary 630, ATR module. Cyclic voltammetry (CV) studies were performed using an ALS/CHI Electrochemical Analyzer 660E. Electrochemical grade NBu_4ClO_4 supplied by Sigma-Aldrich was used as the supporting electrolyte. Electrochemical measurements were performed under nitrogen after the sample solutions were purged with nitrogen for 10 minutes. A glassy carbon disk electrode (GCE; d = 1.6 mm) was used as the working electrode, and a Pt wire as the auxiliary electrode. The non-aqueous Ag-wire reference electrode assembly was filled with 0.01 M $AgNO_3$/0.1 M NBu_4ClO_4/MeCN solution. The reference electrodes were calibrated against ferrocene. The ferrocene peak separation in acetonitrile and CH_2Cl_2 solutions was 105 and 210 mV at 23 °C, respectively.

Methods used for DTF calculations and optimized geometries can be found in Section S4 of the ESI.†

X-ray diffraction data for single crystal samples were collected on a Rigaku XtaLab PRO instrument using graphite mono-chromated MoKα radiation (0.71073 Å) at −180 °C. Fragments of the main residues of complexes **2**, **3** and **6** and anionic

fragments in **3** and **6** were disordered and reported in full in the ESI.† Complex **2** crystallizes as an acetonitrile solvate. Complex **3** contains two independent molecules in the asymmetric cell. Section S5 of the ESI† contains full experimental details regarding data collection and structure refinement.

Results and discussion

Synthesis and structure

Pyridinophane macrocycles can be prepared with various alkyl or functionalized substituents using modifications of known synthetic protocols.[33,46] We produced a set of ligands bearing bulky *tert*-butyl substituents (**L1**) and less bulky ester (**L2**) and alcohol functionalized (**L3**) side chains. In acetonitrile solutions, **L1–L3** rapidly react with $[Cu(MeCN)_4]^+$ precursors to form bright orange solutions of cationic acetonitrile complexes **1–3** (Scheme 1).

Complexes **1–3** readily crystallize to yield analytically pure solids suitable for single crystal X-ray diffraction studies. Fig. 2 shows the solid state structures of these cationic complexes. In all instances the macrocyclic ligand adopts a boat–boat conformation and binds in a κ^4-mode with pyridine units occupying two equatorial positions in the complex with trigonal bipyramidal geometry. We found that the variation of counterion in **1** had little effect of the structure of the complex. Pyridine ligands in the axial plane feature Cu–N distances within 1.9–2.1 Å – common values for pentacoordinate Cu(ɪ) species.[49] As expected, amine donors of all macrocycles occupy axial sites of the bipyramid and have slightly longer Cu–N bonds of *ca.* 2.4 Å.[50] Potentially weaker bonding between the amine donors and the metal in both complexes **1** is manifested in the elongated Cu–N distances in these complexes compared to their less sterically hindered counterparts **2** and **3** ($\Delta > 0.044$ Å).

An intriguing feature of complexes **1–3** in the solid state is the tight placement of the pyridine rings within the macrocyclic ligand that may enable the intramolecular interaction between these aromatic units. Interestingly, the pyridine units of these cationic complexes are packed tighter in complexes with greater steric bulk of the substituents at the amine groups of the macrocycle (Fig. 2). Namely, the 3.475 or 3.495 Å distance between centroids of pyridine units in complexes **1** is *ca.* 0.16–0.18 Å shorter than that in the less sterically hindered complex **2** (3.657 Å). This trend is also associated with a drastic change in the angle formed between the pyridine unit planes – the latter is *ca.* 14% smaller for complexes **1** compared to complex **2**. Taken together, these features suggest that the macrocyclic ligands with high
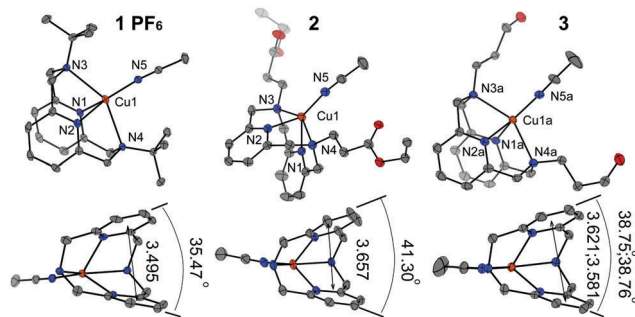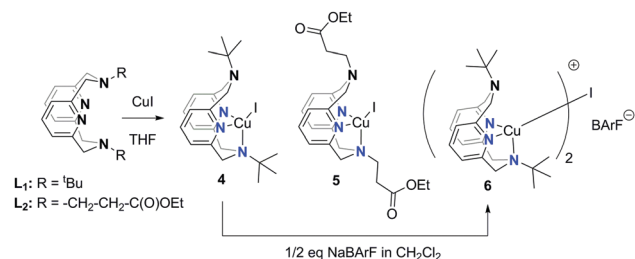

Fig. 2 Solid state structures of cationic Cu complexes **1–3**. Thermal ellipsoids are shown at the 50% probability level; hydrogen atoms, minor disordered fragments, solvent molecules and anions are omitted for clarity. Ring–ring spacing given for centroids; substituents at amine groups are omitted in the side view projections. For complex **3** containing two molecules per asymmetric cell only one molecule is shown. Selected bond lengths and angles (Å, °): **1PF₆**: Cu1–N1 2.089(2), Cu1–N2 2.099(2), Cu1–N3 2.444(2), Cu1–N4 2.470(2), Cu1–N5 1.901(2), N1–Cu1–N2 80.38(9); **2**: Cu1–N1 2.084(2), Cu1–N2 2.048(2), Cu1–N3 2.341(2), Cu1–N4 2.400(2), Cu1–N5 1.869(2), N1–Cu1–N2 82.71(8); **3**: Cu1a–N1a 2.0770(17), Cu1a–N2a 2.1006(17), Cu1a–N3a 2.3687(17), Cu1a–N4a 2.3963(17), Cu1a–N5a 1.8840(18), N1a–Cu1a–N2a 82.13(6).

steric hindrance at amine donors allow for shorter intramolecular contacts between pyridine units that can enhance their interaction. Although the characteristic distance between the centroids of two pyridine units in complexes **1–3** is longer than that in the free **L1** (Fig. 1), only a few known complexes of *N,N*-dialkyl-2,11-diaza[3.3](2,6)-pyridinophane complexes have been reported to have similar Py–Py distances.[51–53]

In an attempt to further alter the intramolecular contact between aromatic units within Cu complexes we aimed at changing the coordination geometry at the metal center. In copper complexes, this can be done by utilizing soft donor ligands that promote the formation of tetrahedral complexes where the pyridinophane ligand would be present in a boat–chair conformation. Indeed, the reactions of copper iodide with ligands **L1** and **L2** (Scheme 2) rapidly resulted in the formation of corresponding iodide complexes **4** and **5** that are readily crystallized as yellow-orange, analytically pure solids. Furthermore, inspired by recent remarkable examples of luminescent compounds based on Cu_2I_2 and Cu_4I_4 cores[30–31,54–56] we attempted the preparation of dinuclear complexes ligated by **L1**. The reaction of complex **4** with 0.5 equivalents of NaBArF as the iodide abstraction agent in dichloromethane resulted in the rapid precipitation of sodium iodide and formation of complex **6** (Scheme 2).
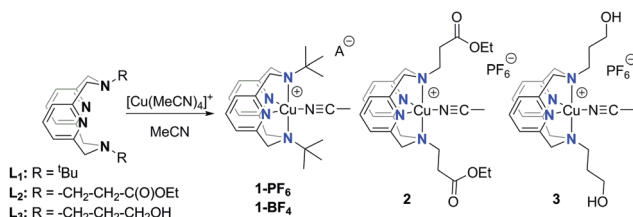
Scheme 1 Synthesis of cationic Cu complexes **1–3**.

Scheme 2 Synthesis of tetragonal halide complexes **4–6**.

1640 | *J. Mater. Chem. C*, 2017, **5**, 1638–1645

This journal is © The Royal Society of Chemistry 2017

X-ray structure analysis confirms the tetrahedral coordination geometry in complexes **4–6**. The macrocyclic ligand in all complexes adopts a boat–chair conformation and binds in a κ^3-fashion with one amine donor group not bound to the copper center. Complexes **4** and **5** have nearly identical Cu1–N3 bond lengths, which implies very similar donor ability of the amine ligands of macrocycles **L1** and **L2**. Consequently, the remote ester group as expected has little effect on the donating strength of the amine group, but rather influences the ligand conformation *via* its reduced steric hindrance. Finally, complex **4** features the shortest distance of 3.349 Å between the centroids of the two pyridine rings among all the complexes studied in this work. The angle between two pyridine rings in **4** is 28.25° that is significantly smaller than the angle in complex **5**, where the pyridine rings are aligned at 43.23° (Fig. 3).

Almost exclusively, the shortest contacts between the aromatic groups of **1–6** in the solid state are intramolecular. For example, the X-ray diffraction data suggest that complexes of **L1** and **L3** have no intermolecular Py–Py contacts in the crystalline state. However, complexes **2** and **5** in solid state demonstrate short intermolecular distances between parallel displaced pyridine units in addition to the intramolecular contacts. The shortest intermolecular Py–Py centroid distances of 3.616 Å (plane shift of 1.572 Å) and 4.740 Å (plane shift of 3.305 Å) were found in **2** and **5**, respectively (see Fig. S52 in the ESI†). Being similar to the intramolecular Py–Py distance, these structural features may potentially impact the properties of crystalline **2** and **5**.

The comparison of the infrared spectra of solid samples complexes **5** and **2** show the presence of a C=O stretching band at 1718 cm^{-1} and 1722 cm^{-1}, respectively, typical for the carbonyl group of aliphatic esters. The IR spectra of cationic complexes **1PF$_6$**, **2**, and **3** exhibit a strong band at ∼830 cm^{-1}, corresponding to a non-coordinated PF$_6^-$ counterion. At the same time, complex **1BF$_4$** features strong bands at 1045 cm^{-1} and 1030 cm^{-1} due to the presence of the BF$_4$ counteranion, while the region between 1650 cm^{-1} and 1410 cm^{-1} corresponding to

pyridine ring vibrations remains essentially unchanged as compared to **1PF$_6$**. In addition, complex **3** featuring OH groups exhibits free and hydrogen-bound OH stretching vibrations at 3593 cm^{-1} and a broad band at ∼3416 cm^{-1}, respectively.

Complexes 1–6 in solution

Having observed remarkable differences in the structural properties of **1–6** in the solid state we further studied how these differences are manifested in solution using NMR spectroscopy. Upon complexation with [Cu(MeCN)$_4$]$^+$ the geminal protons of pyridylmethylenic groups in **L1–L3** lose equivalency and appear in ^{1}H NMR spectra at δ 4.65 and 3.43 ppm in CD$_3$CN as two doublets with $^2J_{HH}$ = 15.2 Hz (see Section S2 of the ESI†). The macrocyclic ligand in complexes **2** and **3** coordinates exclusively in the κ^4-fashion that is evidenced by the C_{2v} symmetry within the ligand moiety observed by ^{1}H NMR spectroscopy at 23 °C. Unlike **2** and **3**, complexes **1BF$_4$** and **1PF$_6$** feature broad resonances in ^{1}H NMR spectra at 23 °C that resolve at −5 °C. Interestingly, a minor isomer with a κ^3 binding mode could be observed in complexes **1BF$_4$** and **1PF$_6$** in a κ^3/κ^4 = 28.5/71.5 ratio. This conformation is easily distinguished from its κ^4 counterpart owing to the loss of symmetry within the macrocyclic ligand. Namely, the two pyridine backbone protons at *meta* positions appear as separate doublets and pyridylmethylenic protons appear as four doublets with different coupling constants $^2J_{HH}$ of 13 and 15.2 Hz in CD$_3$CN. We attribute this behaviour of **L1**-ligated complexes to the increased steric hindrance imposed by *tert*-butyl substituents that may hinder the formation of the κ^4 isomer and lead to the observed exchange.

In agreement with the X-ray diffraction data, the ^{1}H NMR analysis of iodide complexes **4–6** confirms their tetrahedral geometry in CD$_2$Cl$_2$ solution (see ESI†). This can be deduced from a distinct change in the ligand backbone symmetry in solution when compared to complexes **1–3** described above. Namely, the pyridine backbone protons in complex **4** appear as a sharp triplet at δ = 7.25 ppm corresponding to the proton at the *para* position, while *meta*-H resonances appear as a broad feature at room temperature. At −35 °C it resolves into two doublets at δ = 6.86 and 6.65 ppm with identical $^3J_{HH}$ = 7.7 Hz. Methylene groups on the macrocycle appear as four doublets consistent with a C_s symmetric structure. Two separate signals are also observed for N^{t}Bu groups. The ^{1}H NMR spectrum of **6** is nearly identical to that of **4** with the exception of resonances of BArF counterion appearing as singlets at δ = 7.71 and 7.54 ppm.

Interestingly, complexes **4–6** are dynamic on the NMR timescale and their resonances are broadened at 23 °C. While the dynamics in **4** and **6** does not involve changes in the coordination mode of the ligand, complex **5** in dichloromethane solution exists as a mixture of a major tetrahedral complex and a minor trigonal bipyramidal complex in a 61/39 ratio at −35 °C. Resonances of complex **5** in ^{1}H NMR coalesce at *ca.* 10 °C, suggesting a higher exchange rate in CD$_2$Cl$_2$ in **5** compared to complex **4** with a coalescence temperature of 25 °C (see Fig. S27 and S32 in the ESI†).

Conformational equilibria in acetonitrile solutions of **1** and **2** can also be readily observed using cyclic voltammetry when
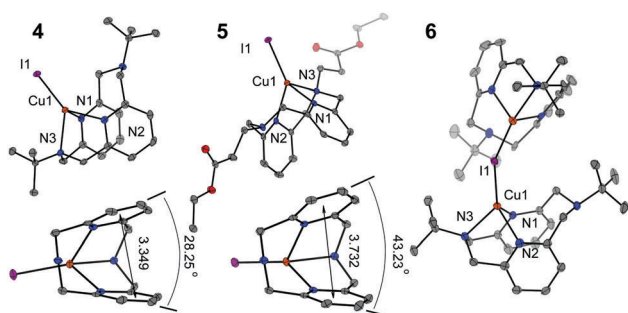

Fig. 3 Solid state structures of neutral Cu complexes **4**, **5** and **6**. Thermal ellipsoids are shown at the 50% probability level; hydrogen atoms, minor disordered fragments and BArF anion in **6** are omitted for clarity. Ring–ring spacing given for centroids; substituents at amine groups are omitted in the side view projections. Selected bond lengths and angles (Å, °): **4**: Cu1–N1 2.1292(16), Cu1–N2 2.1518(15), Cu1–N3 2.2158(16), Cu1–I1 2.4907(3), N1–Cu1–N2 78.64(6); **5**: Cu1–N1 2.1153(16), Cu1–N2 2.0887(17), Cu1–N3 2.2235(16), Cu1–I1 2.4711(3), N1–Cu1–N2 81.63(6); **6**: Cu1–N1 2.0812(13), Cu1–N2 2.1395(14), Cu1–N3 2.2153(13), Cu1–I1 2.4904(2), N1–Cu1–N2 80.12(5).
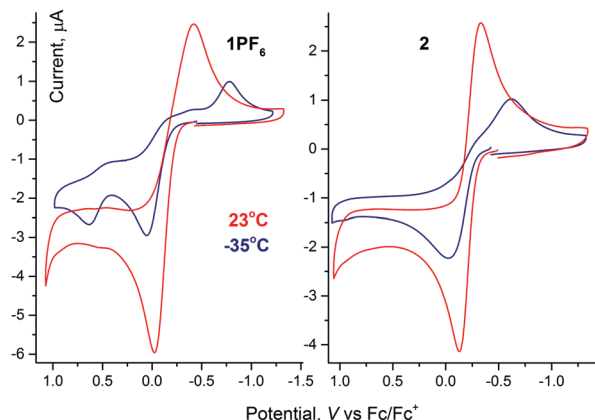
This journal is © The Royal Society of Chemistry 2017

J. Mater. Chem. C, 2017, **5**, 1638–1645 | **1641**

Fig. 4 Cyclic voltammograms of solutions of complexes **1PF$_6$** (1 mM) and **2** (1.2 mM) in 0.1 M NBu$_4$ClO$_4$/CH$_3$CN at 23 °C and −35 °C. Scan rate 100 mV s^{-1}; 1.6 mm glassy carbon disk electrode.

the temperature is varied. At 23 °C, both **1PF$_6$** and **2** show an oxidation wave in MeCN solution with a large separation between anodic and corresponding reverse cathodic waves (Fig. 4). Similar $E_{1/2}$ = −222.5 mV and −229.5 mV vs. Fc/Fc$^+$ measured at 23 °C for complexes **1PF$_6$** (Fig. 4, left, red line) and **2** (Fig. 4, right, red line), respectively, implies that the electronic properties of the remote ester functional group do not significantly affect the electronics at the metal center. In line with the NMR data that suggest the existence of two conformations in **1PF$_6$**, at −35 °C this complex features two oxidation waves, at 59 and 640 mV vs. Fc/Fc$^+$, assigned to the species with κ^4- and κ^3-bound ligands, respectively (Fig. 4).[50] By contrast, complex **2**, shown to exist as a single conformer in solution by ^{1}H NMR spectroscopy correspondingly revealed a single oxidation event even at −35 °C (Fig. 4).

Photophysical studies

Complexes **1–6** absorb light in the near UV region in the solid state. Microspectrophotometry analysis of crystalline samples revealed broad absorption bands in the 300–500 nm range with peak maxima of ca. 395–420 nm (see Fig. S37 in the ESI†). When dissolved in CH$_3$CN or CH$_2$Cl$_2$, complexes **1–6** feature similar intense absorption bands in the deep UV region at 250–300 nm associated with ligand π–π* transitions and less intense broad metal-to-ligand charge-transfer bands at 395–400 nm (see Fig. 5 and Fig. S38 in the ESI†). The free ligands **L1–L3** shows similar π–π* transitions at 260–270 nm, having negligible absorption above 300 nm (see Fig. S37 in the ESI†).

Upon irradiation with 400 nm light, complexes **1–6** emit visible light in the solid state. The emission colour varied from red to green depending on the complex used. While cationic complexes **1–3** emit red light at 619 (identical for **1PF$_6$** and **1BF$_4$**), 637 (**2**) and 665 (**3**) nm, the neutral iodide complexes emit light at 585 (**4**), 564 (**5**) and 524 (**6**) nm (Fig. 6A). The photoluminescence lifetimes determined by time-resolved photoluminescence measurements were in the range of 2–30 μs (see Table 1).

Interestingly, complex **5** had a distinctly different photoluminescence decay profile in the crystalline state (see Fig. S41 in the ESI†). Unlike its counterparts, complex **5** was found to
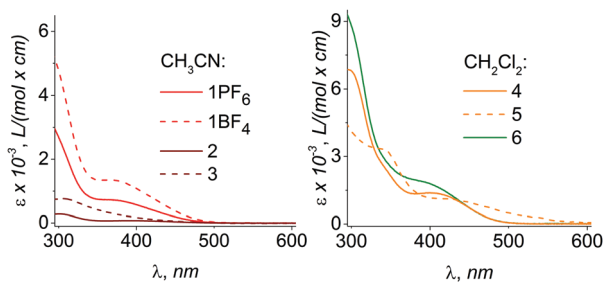

Fig. 5 UV-Vis absorbance spectra of complexes **1–6** in dichloromethane and acetonitrile solutions in the 300–600 nm region.
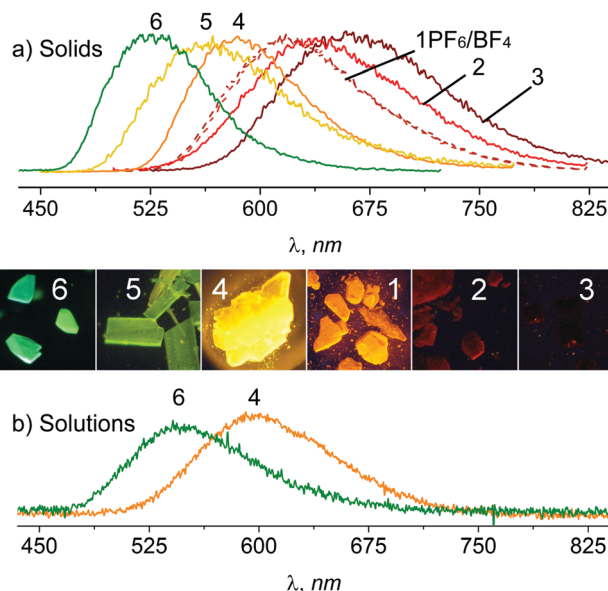

Fig. 6 Normalized emission spectra of complexes **1–6** in solid state (a) and in CH$_2$Cl$_2$ solution (b) at T = 23 °C; excitation at 400 nm. Photographs of crystalline samples are taken with 365 nm light excitation.

have two decay components in the crystalline state with lifetimes of τ = 0.97 and 6.59 μs. Such a behaviour in crystalline **5** can occur due to intermolecular interactions, i.e. the formation of excimers, which is consistent with our X-ray diffraction studies showing relatively short intermolecular Py–Py distances (Fig. S52 in the ESI†) (vide supra). We found that the emission of the long-lived component was significantly red-shifted compared to the short-lived component (Fig. S44 in the ESI†). To assign the decay components to a particular state of complex **5** we analysed the emission of amorphous **5** blended into a PMMA film where the formation of excimers would be less favourable. We found that amorphous **5** emits at λ_{max} = 610 nm that is ca. 45 nm red-shifted from the emission of crystalline **5**. We, therefore, conclude that a long-lived red-shifted component is produced by monomeric **5** rather than its excimers. Interestingly, complex **2**, the cationic counterpart of **5**, features a simple monoexponential decay suggesting that the presence of intermolecular aggregation does not necessarily contribute to emission.

The absolute luminescence quantum yield of copper complexes varied significantly from 0.02 to 0.78. Interestingly, the quantum

1642 | *J. Mater. Chem. C*, 2017, **5**, 1638–1645

This journal is © The Royal Society of Chemistry 2017

Table 1 Summary of absorption and emission characteristics of complexes **1–6** in the crystalline state

Complex	λ_{emi}, nm	CIE color coordinates $(x,y)^g$	Φ^a	τ, μs	k_{rad}, 10^{-3} s^{-1}	d_{Py-Py},^{b} Å
1PF$_6$	619	0.5938,0.4043	0.35	30.05	11.64	3.4950(16)
1BF$_4$	619	0.5889,0.4093	0.30	24.79	12.10	3.4752(12)
2	637	0.6036,0.3940	0.03	18.20	1.77	3.6568(13)
3	665	0.6486,0.3507	0.02	2.63	9.46	3.6211(12) and 3.5806(12)^e
4	585	0.5142,0.4756	0.78	15.79	49.40	3.3494(10)
5	564	0.4388,0.5375	0.08	2.31^c	34.63^d	3.7315(12)
6	524	0.2798,0.5906	0.53	13.90	38.13	3.4647(11) and 3.595(7)/3.611(8)^f

^{a} Absolute quantum yield, all measurements performed with excitation at 400 nm. ^{b} Solid state distance between centroids built on pyridine units. ^{c} Weighted average value derived from the two-component fitting, see Section S2 in the ESI for decay profiles. ^{d} Calculated using the weight averaged lifetime value. ^{e} Values for the symmetrically independent molecules A and B, respectively. ^{f} Values for the first unit and both disordered components of the second unit of binuclear complex **6**, respectively. ^{g} CIE 1931, chromaticity diagram containing solid and solution state data can be found in Fig. S46 of the ESI.

yield and the spatial arrangement of the pyridine rings within the ligand were correlated: complexes with tight intramolecular distances between two pyridine rings were more efficient emitters. Namely, cationic pentacoordinate complexes **1BF$_4$** and **1PF$_6$** that have tight pyridine–pyridine distances have a quantum yield that is at least 10-fold higher than that of analogous complexes **2** and **3**. The same trend is observed in iodide complexes **4**, **6** and **5** where the latter has the longest pyridine–pyridine centroid distance and the lowest corresponding quantum yield.

Much to our satisfaction, the impact of intramolecular interactions in complexes **4** and **6** is sufficient to enable photoluminescence even in solution. Complex **4** emits yellow-orange light (CIE (0.527,0.4512)) at 600 nm in dichloromethane with an absolute quantum yield of 0.28 (Fig. 6B). Its halide-bridged counterpart **6** emits green light (CIE (0.3719,0.5375)) at 545 nm with a quantum yield of 0.15. Interestingly, the emission integral intensity and absorbance of **4** and **6** are directly proportional to their concentration (see Fig. S43 in the ESI†) confirming their nature as molecular emitters that are unaffected by intermolecular forces. Furthermore, solution-like emission characteristics were observed for PMMA films containing complexes **4** and **6**. Very marginally affected by a change in the aggregation state, films containing **4** emit at 580 nm with a quantum yield of 0.29 and films fabricated with complex **6** emit with Φ = 0.26 at 548 nm (see Fig. S45 in the ESI†).

The emission lifetime of complexes **4** and **6** in dichloromethane is considerably lower than that in the solid state. Time resolved photoluminescence spectroscopy measurements estimate the lifetimes to be 4.3 μs for complex **4** and 0.9 μs for complex **6** in CH_2Cl_2. We attribute the lifetime decrease to the prevalence of nonradiative relaxation pathways expected to take effect in solution. Namely, chemical exchange associated with the solution dynamics of the pyridinophane macrocycle may be one of the major contributors to the nonradiative relaxation.

On the origin of the emission

Our structural and photophysical data suggest that intramolecular Py–Py interactions have a crucial effect on the emissive properties of pyridinophane complexes. In this respect, it is particularly important to reveal the electronic transitions involved in photoluminescence. Choosing complex **4** as the representative example, we analyzed its electronic structure

using DFT calculations to identify the photophysical events leading to emission.

Frontier orbital analysis shows that the HOMO in **4** in the ground state is confined mainly to Cu and I centers (57% and 23%, Fig. 7A) with a lower energy HOMO−1 having a similar character. The spatially separated pyridine rings are directly involved in the formation of the excited S$_1$ state of complex **4** since they form the LUMO set that is confined to both pyridine rings (44% and 48% for Py units in the LUMO, Fig. 6A). Interestingly, parts of the LUMO confined to different Py rings have a positive overlap, therefore, the population of the LUMO should enhance the interaction between the Py units.

TD-DFT analysis predicts the S$_0$–S$_1$ transition to have a mixed metal-to-ligand and halide-to-ligand charge-transfer (M + X)LCT character associated with calculated absorption at 385 nm. In agreement with theoretical prediction the lowest energy absorption band was experimentally observed at 400 nm, a common value for MLCT/XLCT bands in Cu complexes.[17] The nature and localization of the LUMOs that are populated upon excitation are the major factors governing the emission. When the LUMO set is populated during excitation one would expect strong attractive forces to emerge that, in turn, should alter the geometry of the excited state. Indeed, the TD-DFT analysis indicates the contraction of the Py–Py spacing by Δ = 0.25 Å upon the formation of the first excited state S$_1$ (Fig. 6B).

As the emission lifetimes observed for complex **4** are relatively long (15.79 μs in the solid state and 4.3 μs in solution), the possible contribution of the triplet state to overall emission is likely. In agreement with this suggestion, DFT analysis estimates the emission maxima for the triplet state at 614 nm, while the S$_1$ state would emit at 557 nm. Interestingly, the relaxation of the T$_1$ state geometry that precedes the emission is also associated with the rearrangement of the stacking pyridine units within **4**. Similarly to S$_1$, the T$_1$ state has significantly shorter Py–Py contacts compared to the ground state (Δ = 0.23 Å). As expected, the formation of the T$_1$ state strengthens the interaction between the Py units in the macrocyclic ligand as evidenced by the frontier orbital analysis. Namely, the population of the LUMO level in S$_0$ results in the formation of a new SOMO of T$_1$ featuring a positive overlap between the Py units (Fig. 6A). Similarly to the LUMO of S$_0$, the higher energy SOMO of T$_1$ is almost exclusively confined to pyridine units (52 and 41% for each Py unit). This, in turn,
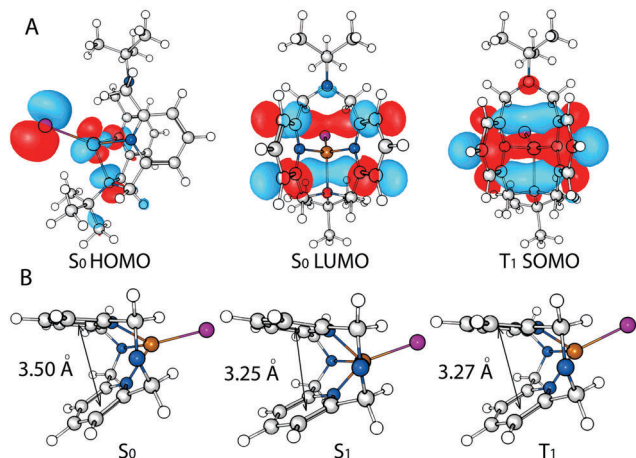
Fig. 7 DFT computed (A) frontier HOMO/LUMOs of complex **4** in the ground state S_0 and the highest populated SOMO of the T_1 state in CH_2Cl_2 at an isosurface value 0.03 and (B) optimized structures of S_0, S_1 and T_1 states. ^{t}Bu substituents omitted for clarity, the values indicated correspond to the distances between centroids built on pyridine units.

suggests stronger bonding between the Py units in T_1 compared to the ground state.

In summary, pyridine units in complex **4** not only interact but directly influence its emissive properties in two ways. Firstly, they provide electron accepting LUMOs in the ground state (S_0) confined exclusively to the pyridine units. Secondly, the interaction between pyridine units strengthens upon excitation and directs the formation of stable geometries of excited S_1 and T_1 states – the crucial step that precedes emission.

Conclusion

In conclusion, we have developed a new class of transition metal-based compounds that rely on intramolecular non-covalent interactions to enable photoluminescence. In contrast to the majority of emissive TM complexes that are tuned *via* modification of the donor/acceptor properties of their ligand, the compounds reported in this work are tuned by the variation of *steric* properties of macrocyclic ligands that impacts the intramolecular non-covalent interactions within the ligand molecule.

As a result, simple pyridinophane macrocycles act as potent and tunable ligands that yield copper(ı) complexes emitting in the range of 524–665 nm with a quantum yield up to 78% at 23 °C. Due to the molecular nature of the emission, complexes **4** and **6** are capable of solution state emission with quantum yields of 28 and 15% correspondingly. Our experimental data suggest a strong link between the extent of intramolecular aromatic interaction and the photoluminescence quantum yield and DFT calculations explain how these interactions are involved in the formation of emissive states. Finally, our results introduce a new strategy for designing photoluminescent compounds that employs subtle conformational modifications as the main tuning motif. Being intrinsically sensitive to the local steric environment, the new emissive complexes hold a good potential to be utilized in sensing and imaging applications.

Notes and references

1 R. C. Evans, P. Douglas and C. J. Winscom, *Coord. Chem. Rev.*, 2006, **250**, 2093–2126.
2 J. Wu, W. Liu, J. Ge, H. Zhang and P. Wang, *Chem. Soc. Rev.*, 2011, **40**, 3483–3495.
3 K. Li, W. Qin, D. Ding, N. Tomczak, J. Geng, R. Liu, J. Liu, X. Zhang, H. Liu, B. Liu and B. Z. Tang, *Sci. Rep.*, 2013, **3**, 1150.
4 Z. Wang, J. Nie, W. Qin, Q. Hu and B. Z. Tang, *Nat. Commun.*, 2016, **7**, 12033.
5 S. Lee, S.-O. Kim, H. Shin, H.-J. Yun, K. Yang, S.-K. Kwon, J.-J. Kim and Y.-H. Kim, *J. Am. Chem. Soc.*, 2013, **135**, 14321–14328.
6 F. Julia, D. Bautista, J. M. Fernandez-Hernandez and P. Gonzalez-Herrero, *Chem. Sci.*, 2014, **5**, 1875–1880.
7 X. Yan, T. R. Cook, P. Wang, F. Huang and P. J. Stang, *Nat. Chem.*, 2015, **7**, 342–348.
8 R. Sakamoto, T. Iwashima, J. F. Kögel, S. Kusaka, M. Tsuchiya, Y. Kitagawa and H. Nishihara, *J. Am. Chem. Soc.*, 2016, **138**, 5666–5677.
9 T. Seki, Y. Takamatsu and H. Ito, *J. Am. Chem. Soc.*, 2016, **138**, 6252–6260.
10 D. Volz, M. Wallesch, C. Flechon, M. Danz, A. Verma, J. M. Navarro, D. M. Zink, S. Brase and T. Baumann, *Green Chem.*, 2015, **17**, 1988–2011.
11 N. Armaroli, G. Accorsi, F. O. Cardinali and A. Listorti, *Photochemistry and Photophysics of Coordination Compounds I*, Springer Berlin Heidelberg, Berlin, Heidelberg, 2007, vol. 280, pp. 69–115.
12 P. C. Ford, E. Cariati and J. Bourassa, *Chem. Rev.*, 1999, **99**, 3625–3648.
13 A. l. Lavie-Cambot, M. Cantuel, Y. Leydet, G. Jonusauskas, D. M. Bassani and N. D. McClenaghan, *Coord. Chem. Rev.*, 2008, **252**, 2572–2584.
14 O. Horváth, *Coord. Chem. Rev.*, 1994, **135**, 303–324.
15 T. Hofbeck, U. Monkowius and H. Yersin, *J. Am. Chem. Soc.*, 2015, **137**, 399–404.
16 S. B. Harkins and J. C. Peters, *J. Am. Chem. Soc.*, 2005, **127**, 2030–2031.
17 A. Tsuboyama, K. Kuge, M. Furugori, S. Okada, M. Hoshino and K. Ueno, *Inorg. Chem.*, 2007, **46**, 1992–2001.
18 M. Nishikawa, Y. Wakita, T. Nishi, T. Miura and T. Tsubomura, *Dalton Trans.*, 2015, **44**, 9170–9181.
19 D. R. McMillin and K. M. McNett, *Chem. Rev.*, 1998, **98**, 1201–1220.

20 G. Blasse and D. R. McMillin, *Chem. Phys. Lett.*, 1980, **70**, 1–3.

21 D. G. Cuttell, S.-M. Kuang, P. E. Fanwick, D. R. McMillin and R. A. Walton, *J. Am. Chem. Soc.*, 2002, **124**, 6–7.

22 C. Bizzarri, C. Strabler, J. Prock, B. Trettenbrein, M. Ruggenthaler, C.-H. Yang, F. Polo, A. Iordache, P. Braggeller and L. D. Cola, *Inorg. Chem.*, 2014, **53**, 10944–10951.

23 M. Nishikawa, T. Sano, M. Washimi, K. Takao and T. Tsubomura, *Dalton Trans.*, 2016, **45**, 12127–12136.

24 V. A. Krylova, P. I. Djurovich, M. T. Whited and M. E. Thompson, *Chem. Commun.*, 2010, **46**, 6696–6698.

25 V. A. Krylova, P. I. Djurovich, J. W. Aronson, R. Haiges, M. T. Whited and M. E. Thompson, *Organometallics*, 2012, **31**, 7983–7993.

26 V. A. Krylova, P. I. Djurovich, B. L. Conley, R. Haiges, M. T. Whited, T. J. Williams and M. E. Thompson, *Chem. Commun.*, 2014, **50**, 7176–7179.

27 R. Marion, F. Sguerra, F. Di Meo, E. Sauvageot, J.-F. o. Lohier, R. Daniellou, J.-L. Renaud, M. Linares, M. Hamel and S. Gaillard, *Inorg. Chem.*, 2014, **53**, 9181–9191.

28 A. J. M. Miller, J. L. Dempsey and J. C. Peters, *Inorg. Chem.*, 2007, **46**, 7244–7246.

29 K. J. Lotito and J. C. Peters, *Chem. Commun.*, 2010, **46**, 3690–3692.

30 Y. Okano, H. Ohara, A. Kobayashi, M. Yoshida and M. Kato, *Inorg. Chem.*, 2016, **55**, 5227–5236.

31 H. Araki, K. Tsuge, Y. Sasaki, S. Ishizaka and N. Kitamura, *Inorg. Chem.*, 2005, **44**, 9667–9675.

32 C. T. Cunningham, K. L. H. Cunningham, J. F. Michalec and D. R. McMillin, *Inorg. Chem.*, 1999, **38**, 4388–4392.

33 C.-M. Che, Z.-Y. Li, K.-Y. Wong, C.-K. Poon, T. C. W. Mak and S.-M. Peng, *Polyhedron*, 1994, **13**, 771–776.

34 J. Mei, N. L. C. Leung, R. T. K. Kwok, J. W. Y. Lam and B. Z. Tang, *Chem. Rev.*, 2015, **115**, 11718–11940.

35 Y. Hong, J. W. Y. Lam and B. Z. Tang, *Chem. Commun.*, 2009, 4332–4353.

36 X. Zhang, Z. Chi, Y. Zhang, S. Liu and J. Xu, *J. Mater. Chem. C*, 2013, **1**, 3376–3390.

37 T. U. Connell, J. M. White, T. A. Smith and P. S. Donnelly, *Inorg. Chem.*, 2016, **55**, 2776–2790.

38 Q. Zhao, L. Li, F. Li, M. Yu, Z. Liu, T. Yi and C. Huang, *Chem. Commun.*, 2008, 685–687.

39 G.-G. Shan, H.-B. Li, H.-Z. Sun, D.-X. Zhu, H.-T. Cao and Z.-M. Su, *J. Mater. Chem. C*, 2013, **1**, 1440–1449.

40 K. Huang, H. Wu, M. Shi, F. Li, T. Yi and C. Huang, *Chem. Commun.*, 2009, 1243–1245.

41 Y. You, H. S. Huh, K. S. Kim, S. W. Lee, D. Kim and S. Y. Park, *Chem. Commun.*, 2008, 3998–4000.

42 M. Osawa, *Chem. Commun.*, 2014, **50**, 1801–1803.

43 R.-H. Wei, J.-F. Chen, J.-Q. Feng, J.-S. Hu and D.-K. Cao, *RSC Adv.*, 2015, **5**, 14359–14365.

44 J. R. Khusnutdinova, N. P. Rath and L. M. Mirica, *Inorg. Chem.*, 2014, **53**, 13112–13129.

45 S. P. Meneghetti, P. J. Lutz and J. Kress, *Organometallics*, 2001, **20**, 5050–5055.

46 F. Bottino, M. Di Grazia, P. Finocchiaro, F. R. Fronczek, A. Mamo and S. Pappalardo, *J. Org. Chem.*, 1988, **53**, 3521–3529.

47 N. A. Yakelis and R. G. Bergman, *Organometallics*, 2005, **24**, 3579–3581.

48 G. J. Kubas, B. Monzyk and A. L. Crumblis, *Inorganic Syntheses*, John Wiley & Sons, Inc., 2007, pp. 68–70.

49 S. Holler, M. Tüchler, F. Belaj, L. F. Veiros, K. Kirchner and N. C. Mösch-Zanetti, *Inorg. Chem.*, 2016, **55**, 4980–4991.

50 J. R. Khusnutdinova, J. Luo, N. P. Rath and L. M. Mirica, *Inorg. Chem.*, 2013, **52**, 3920–3932.

51 W.-T. Lee, S. B. Muñoz, D. A. Dickie and J. M. Smith, *Angew. Chem., Int. Ed.*, 2014, **53**, 9856–9859.

52 W. O. Koch and J. T. Kaiser, *Chem. Commun.*, 1997, 2237–2238.

53 M. Jagoda, S. Warzeska, H. Pritzkow, H. Wadepohl, P. Imhof, J. C. Smith and R. Krämer, *J. Am. Chem. Soc.*, 2005, **127**, 15061–15070.

54 K. Tsuge, *Chem. Lett.*, 2013, **42**, 204–208.

55 S. Perruchas, X. F. Le Goff, S. Maron, I. Maurin, F. Guillen, A. Garcia, T. Gacoin and J.-P. Boilot, *J. Am. Chem. Soc.*, 2010, **132**, 10967–10969.

56 M. Vitale and P. C. Ford, *Coord. Chem. Rev.*, 2001, **219–221**, 3–16.